A Test of Fast Switching Phase Calibration With The VLA at 22 GHz

M.A. Holdaway and F.N. Owen
National Radio Astronomy Observatory
Socorro, NM 87801

April 18, 1995

Abstract

We have performed a limited demonstration of the fast switching phase calibration technique using the VLA in C array at 22 GHz. Using a calibration cycle time of 80 s and two bright calibrators about 2° apart on the sky, we were able to track short time scale fluctuations and improve the phase on baselines longer than about 400 m. We find that the residual (ie, post calibration) phase errors follow the phase structure function for baselines less than $vt/2 + d$, and are constant and consistent with $\sqrt{D_\phi(vt/2 + d)}$ and $v = 10\ m/s$ for longer baselines. These residual phase errors are actually smaller than predicted by Holdaway (1992). The improvements come from using half the cycle time to estimate the phase errors on the target source.

Updated estimates of how well fast switching will work for the MMA on Mauna Kea indicate that observing at 230 GHz will not be limited by phase errors about 75% of the time, that calibrators down to about 0.05 Jy can be used, and that a large increase in bandwidth (from 2 GHz to 10 GHz total bandwidth) improves the effectiveness of fast switching phase calibration but is not required.

1 Introduction

It has long been recognized that phase calibration on long baselines and at high frequencies will be problematic for the MMA (Holdaway, 1991). The members of the MDC (Millimeter Array Development Consortium) are currently testing four phase calibration techniques to try to improve this situation:

- the BIMA group is working on deriving the column density of water vapor, and hence the phase fluctuations, from accurate measurements of the T_{sys} fluctuations on each antenna;
- the OVRO group is working on deriving the column density of water vapor from the atmospheric emission at and around the 22 GHz water vapor line;

- the NRAO group is working on fast switching to calibrate the atmospheric phase by observing calibrators a few degrees away from the target source on time scales of 5-10 seconds.

- the NRAO group is also working on solving for a phase screen and applying it to data taken on the target source. The phase screen could be determined by a subarray of the MMA observing a bright calibrator source, or an array of 2 m "site testing" dishes observing satellite beacons at centimeter wavelengths.

At this point in time, we are not certain that any of these methods will satisfactorily meet the calibration needs of MMA, and therefore it is prudent to work on developing all methods.

The theory and rough error analysis of fast switching calibration was developed in Holdaway, 1992. The residual phase errors are related to the atmospheric phase structure function $D_\phi(\rho)$ and parameters of the calibration method by

$$\sigma_\phi = \sqrt{2D_\phi(v_{atmos}t_{cycle} + d)}, \tag{1}$$

where v_{atmos} is the atmospheric velocity, t_{cycle} is the time required to complete one full target source, calibrator source cycle , and d is the distance between the lines of site to the calibrator and to the target source, at the height of the water vapor layer. The residual phase errors are largely random from one solution interval to another, and residual phase errors as large as 30° rms still result in good imaging.

Since the initial work on fast switching, work has gone into quantifying the millimeter wavelength source counts (Holdaway, Owen, and Rupen, 1994) and quantifying the slew rates and settle-down times for the MMA antennas (Cheng, private communication), which are all required to estimate the success of fast switching calibration for MMA observations. This memo presents experimental evidence that fast switching works for the VLA and refines our theoretical understanding of fast switching phase calibration. Also, we further refine our estimates of the success of fast switching for the Mauna Kea site.

2 An Observational Test of Fast Switching

2.1 The Observations

We observed the VLA calibrator sources 2134+004 and 2131-021 (B1950) on 4 December 1994 between LST 20:30 and LST 21:30. We did not perform any flux calibration, but we previous measurements indicate 2134+004 is about 5 Jy and 2131-021 is about 1 Jy. The atmosphere was fairly stable in spite of a thin cloud cover, so we observed at 22 GHz, the highest feasible frequency. We did not consider 43 GHz because the antennas equipped with 43 GHz receivers are all in the inner part of the C array with baselines under 600 m, too short to see the long baseline cutoff in the phase structure function. The observed baselines ranged from 65 m to 3000 m. Data were recorded with a 3.3 s integration time, and we sought to spend 10 s on each source before switching to the other. Even for the case of two consecutive scans on the

same object, the VLA on-line system requires 20 s for set up between scans. In addition, scan changes occur only on a grid with 10 s intervals. This resulted in a cycle time of 80 s, the shortest conceivable cycle time for the VLA at this time. Because the details of the source changes are not fully modeled by the observe program, we usually got about 20 s of data per source per cycle, but sometimes we got only 10 s of data. After the data were obtained, we averaged down to 10 s integration times.

2.2 Residual Phase Errors

The phase structure function could be estimated by looking at all the data on 2131-021. The gaps in time do not present any problem except for the very shortest baselines. On these baselines, the thermal noise in the phase is actually larger than the atmospheric phase anyway. For each baseline, the mean phase for the hour was removed and the rms phase was calculated. The rms phase is then plotted as a function of baseline in Figure 1 to yield the square root of the phase structure function. The rms phase was found to increase approximately as the square root of the baseline. This structure function is not consistent with Kolmogorov turbulence, but has been seen at a number of sites during conditions of very good phase stability (Bester, 1991; Holdaway, 1991). Antenna based gains were calculated for the 2134+004, and the gains were applied to the 2131-021 data. The residual phase structure function for the calibrated 2131-021 data are shown on the same plot as the phase structure function. For baselines less than about 400 m, the phase increases with baseline in the same manner as the phase structure function. For baselines greater than 400 m, the residual rms phase is flat at about 12°. This is consistent with residual phase errors given by

$$\sigma_\phi = \sqrt{D_\phi(v_{atmos} t_{cycle}/2 + d)} \tag{2}$$

with $v_{atmos} = 10\ m/s$, which is significantly more optimistic than our original estimate for the residual phase errors. The factor of 2 in $t_{cycle}/2$ of Equation 2 is understood because it is the phase variation which occurs over time scales of half the cycle time, or the time which elapses between the calibration and the target source observation, by which the phases are in error. The reasoning which led to the $\sqrt{2}$ in Equation 1 was rooted in baseline-based calibration, and it goes away for antenna based calibration.

The residual phase errors follow the structure function on the shortest baselines. Since the lines of site to the calibrator and to the target source are different, and the distance between the lines of site is actually larger than the shortest baselines, we might expect to corrupt the shortest baselines. The gain phases which we determine for each antenna are in fact in error, but the errors are correlated for nearby antennas, and some of the error cancels out when we apply the gains, leaving us with the same rms phase error as the structure function.

Both the raw phase errors in the structure function and the residual phase errors seem to be isotropic: the data show no trends when we look at north-south and east-west baselines separately.

As longer cycle times are used (ie, applying only a subset of the 2134+004 solutions to

2131-021), we find that the baseline beyond which the residual phase errors become constant increases linearly with the cycle time.

Is the 10 m/s wind velocity reasonable? The VLA site is at about 2150 m, and we assume that the bulk of the water vapor is at about 1 km above the VLA. Schwab (1992) has studied the wind velocities above Albuquerque, NM, and finds the median velocity in December to be 12.5 m/s at 3400 m. We might expect the nights with the best phase stability to have somewhat lower wind velocities than the median. However, the night of our observations was not particularly spectacular: 43 GHz observations with a typical calibration strategy would have been only marginally successful. Our 10 m/s wind velocity guess is not inconsistent with what we know about the winds aloft. Furthermore, the temporal structure function is expected to turn over for lag times of about $4 * \rho / v_{atmos}$. Investigation of the longest baselines indicates wind velocities of about 11 m/s.

2.3 Tracking Phase Solutions

The rms phases are the primary observable, but it is reassuring to see how the antenna base gain phases for the two calibrators track. We have solved for the gain phases on both calibrators an displayed them as a function of time. Since the phases of each antenna are referenced to the reference antenna, the gain phases represent the difference of the atmospheric fluctuations above one antenna and the reference antenna. For antennas far from the reference antenna, we expect to see large time variations in the phases, while antennas close to the reference antenna will show small time variations. In Figure 2 we show the antenna gain phases on the two calibrators as a function of time for antenna 7, which is close to the reference antenna, and for antenna 25, which is far away from the reference antenna. For all antennas, the rms difference of gain phases as determined on the two different calibrators is about 13°. Since the gain phases are referenced to the reference antenna, the actual rms of the atmosphere will be better by $\sqrt{2}$.

3 Future Observational Tests

One obvious simple improvement that could be implemented at the VLA for fast switching calibration would be to reduce the 20 s of dead time which occurs between scans even when no hardware or software changes are required. This dead time can be eliminated if the instructions for the switching antenna motion can be specified in an `//OF` offset card, allowing the on-line system to treat the observation as a single scan. The cycle time can probably be reduced to 40 s by using an "//OF" card. Such a test would put us within a factor of four of the MMA's proposed 10 s cycle times.

Further tests need to be done to verify that the residual phase errors are consistent with Equation 2':

- Exceptionally low wind velocities would give rise to lower than expected residual phase errors. Are our lower than expected residual phase errors caused by low wind velocities

during our observations, or by our mistakes in deriving Equation 1?

- Also, we have not investigated the dependence of the residual phase errors on the distance between the calibrator and target source on the sky. In our previous analysis, we sought to minimize the quantity $vt/2 + d$. However, since the cycle time t depends also upon d through the antenna slew rate, the optimal MMA calibration strategy has $vt/2 >> d$. In this regime, the residual phase errors should be independent of the distance between calibrators. When d becomes comparable with $vt/2$, we should note an increase in the residual phase errors. For the 40 s cycle time, a 10 m/s wind velocity, and a 1 km atmosphere, the two terms are comparable for sources about 10° apart on the sky. It would therefore be beneficial to perform fast switching at a fixed cycle time on several calibrator pairs ranging from 2° to 15° separation, during comparable atmospheric condition.

4 VLA Implications

Both the Q band and K band VLA systems could benefit from fast switching in the A, B, C, and possibly D configurations. Since fast switching will result in a factor of ~ 2 higher noise due to the decreased time on source, we need real time phase stability monitoring at the VLA to determine if fast switching is required. An MMA site tipper operating in stability mode would be optimal, but the D10 display on a long baseline observing a bright source for a few minutes would be acceptable.

As mentioned above, a new variety of `//OF` card is required to obtain the shortest possible cycle time at the VLA.

Since the integrations on source are very short, we require 3.3 s integration times. The on-line system may require more work to become robust for 3.3 s integration times.

If the 40 s cycle time is achievable with the new `//OF` card, we would like to be able to move between sources in under 10 s. For moves in azimuth (40°/s slewing), this requires the sources be within 6°. For moves in elevation (20°/s slewing), this requires the sources be within 3°.

How bright must the calibrator source be? Using the A, B, C, and D IFs together to solve for the atmospheric phase, and permitting 12° rms phase errors due to noise on the calibrator in 10 s, we can make use of 250 mJy sources at K band, and weaker sources if larger phase errors are permitted. A project to estimate the 43 GHz source counts is underway. The preliminary source counts indicate that there are enough bright sources on the sky. We already know many of the bright sources at 22-43 GHz. A more complete list of weak and intermediate strength calibrators at K and Q bands is also required.

5 MMA Implications

The distribution of residual phase errors obtained after fast switching phase calibration will result from a combination of the distribution of $vt/2 + d$ and the distribution of $D_\phi(\rho)$. Large

residual phase errors could be due to having no nearby bright calibrators (even if the atmosphere is fairly agreeable) or due to having a disagreeable atmosphere (even if there is a good calibrator very close to the target source).

We make the following assumptions in calculating the distribution of $vt/2 + d$ and the distribution of $D_\phi(\rho)$:

- **Observing Frequencies:** We assumed phase calibration at 90 GHz and target source observations at 230 GHz.

- **Antenna Slew Rate** is about 2°/s on the sky. The slew rates of the two bearings in the slant axis MMA antenna design are each about 3°/s, but the singularities at the zenith (for the azimuth axis) and at the horizon (for the slant axis) cause the actual sky slew rate to be much lower. However, 2°/s is possible in most directions between elevations of 20° and 70°. Because the two axes have singularities at different elevations, the optimal slew direction changes as a function of elevation. Observers may want to use different phase calibrators for high and low elevations to reflect this.

- **Setup Time** is 1 s. We define the setup time as the dead time between when the antennas stop slewing and start observing. The setup time is currently limited by the estimated antenna settle time required to achieve $\sim 5-8''$ pointing errors (Cheng, private communication). While the MMA has a pointing specification of $1''$, this is only required for mosaicing of large objects. Much poorer pointing can be tolerated on compact objects. Since the phase stability in the compact mosaicing configurations will be good there is little need for fast switching.

  The fast setup time also places stringent requirements on the optics, the LO, the IFs, and the correlator: during the slew time to and from the calibrator (which will typically be under a second) and the 1 s setup time, the entire MMA system will be required to switch to a new observing frequency.

- **Target Source Observing Fraction:** We performed calculations spending both 0.33 and 0.67 of the total cycle time integrating on the target source, resulting in a noise increase over full time observing of factors of 1.74 and 1.22 respectively.

- $\mathbf{T_{sys}}$ at 90 GHz was modeled with the following contributions:

  - $T_{bg} = 2.7$ K
  - $T_{spill} = 2$ K (minimized by the off-axis design)
  - $T_{sky} = 263K * (1 - \exp^{-0.01h/\sin(el)})$
  - $T_{rx} + T_{loss} = 40$ K

- **Precipitable Water Vapor** was taken to be 1 mm (used for opacity and T_{sys} only).

- **Antenna Efficiency** was taken to be 0.76, with most of the losses due to feed spill over and illumination taper.

- **Bandwidths** used were 1, 2, and 10 GHz. This is the total bandwidth for two polarizations, and 2 GHz (1 GHz SSB per polarization) is the current MMA spec.

- **Calibrator Distribution.** Using the 90 GHz source counts of Holdaway, Owen, and Rupen (1994), we have used Foster's (1994) Monte Carlo program to simulate distributions of calibrator sources over an 8° squared field.

- **Atmospheric Velocity** on Mauna Kea is believed to be close 5 m/s. We have performed calculations with 5 m/s and 10 m/s.

- **Atmospheric Height** is taken to be 1 km above the array. A water vapor layer which is closer to the array will result in smaller distances between the target source and calibrator source lines of site, resulting in smaller phase errors than those we report.

- **Phase Structure Function:** The distribution of phase structure functions D_ϕ were taken from Colin Masson's SMA site testing results (1992). We assumed that

$$\sqrt{D_\phi} = A\rho^{0.75}, \tag{3}$$

  ρ being the baseline and A being dependent upon the atmospheric conditions. The power 0.75 is approximately the median value for all conditions Masson observed, and the values of A were derived from a graph showing the distribution of rms phase on Masson's 100m baselines. This phase data is taken at a 30° elevation. Masson's data were collected in Millimeter Valley at 13,200 ft, while the potential MMA site is at 12,000 ft, suggesting that the phase stability will be worse at the MMA site. Millimeter Valley has topographical obstructions in most directions. It is possible that these features, including the Mauna Kea summit, may disrupt the laminar airflow and inject turbulence into the atmosphere, thereby degrading the phase stability. There are no topographical obstructions to the prevailing trade wind at the potential MMA site at 12,000 ft, and flow may be less turbulent at this lower site. Hence, the phase stability at the MMA site may be comparable or even better than the stability in Millimeter Valley. The MMA site testing interferometer near the potential MMA site will help clarify the situation.

- **Residual phase errors** were assumed to be

$$\sigma_\phi = \sqrt{D_\phi(v_{atmos}t_{cycle}/2 + d)} \tag{4}$$

Distribution of $vt/2 + d$: We simulated 8° square fields of 90 GHz calibrators ranging in flux from 0.010 Jy to 5 Jy. For each field, we determined the quantity $vt/2 + d$ for each calibrator (for each combination of 1, 2, and 10 GHz total bandwidth, 5 and 10 m/s wind velocity, and 0.33 and 0.67 target source observing fraction) and chose the calibrator with the minimum value of $vt/2+d$. We performed these computations for 600 simulated fields and then computed the probability distribution of $vt/2+d$ for each bandwidth, wind velocity, and target source fraction. The probability distribution of $vt/2 + d$ for bandwidths of 1 GHz, 2 GHz, and

10 GHz, 5m/s atmospheric velocity, and a target source observing fraction of 0.33 is shown in Figure 3. Earlier rough calculations indicated that fast switching would only work to about 100 m, basically providing no phase relief for the 70 and 150 m arrays (which had pretty good phase stability already). However, the distributions of $vt/2 + d$ indicate that fast switching will often be able to help the phase calibration in these small configurations, especially if a wide bandwidth is used. For 2 GHz bandwidth, the mean calibrator flux is 230 mJy, the minimum calibrator flux is about 50 mJy, the mean distance to a calibrator is 0.55 degrees, and the maximum distance to a calibrator is 3.3 degrees. For the 10 GHz bandwidth case, the mean calibrator flux is 180 mJy, the minimum calibrator flux is about 30 mJy, the mean distance to a calibrator is 0.34 degrees, and the maximum distance to a calibrator is 1.64 degrees.

Distribution of residual phase errors: From the probability distribution of $vt/2 + d$ and the distribution of phase structure function coefficients, we can estimate the cumulative distribution of residual phase errors (ie, the fraction of time which fast switching will result in residual phase errors less than some value). The value of the residual phase error which is required will depend upon the demands of each individual experiment, but we assert that 30° residual phase errors will be adequate for many experiments. We show the cumulative distribution of residual phase errors for all phase conditions on Mauna Kea in Figure 4 (0.33 target source fraction, 5 m/s wind velocity). This indicates that fast switching will work about 75% of the time with 2 GHz bandwidth, and about 85% of the time with 10 GHz bandwidth (not discounting any times when observations may not be possible at all because of dramatic amplitutde fluctuations due to inhomogeneously distributed water *droplets*). The RMS phase errors at the very low end of these plots are being underestimated because we have observed the calibrators only long enough to measure the phase to an accuracy of 10° rms. We show similar plots for the cumulative distribution of the residual phase for the best 50% of the phase conditions and the best 25% of the phase conditions in Figures 5 and 6. These figures demonstrate that fast switching should work very well when the really poor atmospheric conditions are excluded. When we increased the velocity from 5 m/s to 10 m/s in the computations, the curves are shifted to higher residual phase errors by a factor of about 1.5 (not shown). The phase errors did not increase by the full factor of two because of the d term in $vt/2 + d$, which is comparable to the $vt/2$. If the target source observing fraction is 0.67, the residual phase error curves are shifted higher by a factor of about 1.5 (see Figure 7). Comparison with the 0.33 observing fraction curves indicate that spending 0.33 of the time on the target source and using 1 GHz bandwidth on the calibrator is about the same as spending 0.67 of the time on the target source and using 10 GHz bandwidth on the calibrator. Hence, the extra bandwidth may be justified in that it allows more time to be spent on the target source.

6 References

1. Bester, M., Danchi, W.C., Degiacomi, C.G, Greenhill, L.J., and Townes, C.H., *ApJ*, 1991.
2. Cheng, Jingquan, 1994, private communication.

3. Foster, Scott M., 1994, "(Angular) Distances to MMA Calibrators Based on 90 GHz Source Counts", MMA Memo 124.
4. Holdaway, M.A., 1991, "A Millimeter λ Phase Stability Analysis of the South Baldy and Springerville Sites", MMA Memo 68.
5. Holdaway, M.A., 1992, "Possible Phase Calibration Schemes for the MMA", MMA Memo 84.
6. Holdaway, M.A., Owen, F.N., and Rupen, M.P. 1994, "90 GHz Source Counts", MMA Memo 123.
7. Masson, Colin, 1992, from a handout and talk presented at the SMA design review.
8. Schwab, F.R., 1992, "Lower Tropospheric Wind Speed Statistics...", MMA Memo 75.

Figure 1: Phase structure function for the uncalibrated phases on the source 2131-021 and the structure function of the residual phase errors after calibrating every 80 s on the nearby source 2134+004.

Figure 2: How do the phase solutions on the nearby calibrators track each other? a: the phases of the gain solutions from 2134+004 and 2131-021 for antenna 25 (about 1800 m from the reference antenna). b: and for antenna 7 (about 360 m away from the reference antenna).

Figure 3: Simulated probability distributions for $vt/2 + d$ for a target source observing fraction of 0.33, a wind velocity of 5 m/s, and 1 GHz (solid line), 2 GHz (dotted line), and 10 GHz (dashed line) total (both polarizations combined) bandwidth cases.

Figure 4: Cumulative distribution of residual phase errors for fast switching considering *all atmospheric conditions* on Mauna Kea, a target source observing fraction of 0.33, a wind velocity of 5 m/s, and 1 GHz (solid line), 2 GHz (dotted line), and 10 GHz (dashed line) total (both polarizations combined) bandwidth cases.

Figure 5: Cumulative distribution of residual phase errors for fast switching considering *the best half* of the atmospheric conditions on Mauna Kea, a target source observing fraction of 0.33, a wind velocity of 5 m/s, and 1 GHz, 2 GHz, and 10 GHz total (both polarizations combined) bandwidth cases.

Figure 6: Cumulative distribution of residual phase errors for fast switching considering *the best quarter* of the atmospheric conditions on Mauna Kea, a target source observing fraction of 0.33, a wind velocity of 5 m/s, and 1 GHz, 2 GHz, and 10 GHz total (both polarizations combined) bandwidth cases.

Figure 7: Cumulative distribution of residual phase errors for fast switching considering the best half of the atmospheric conditions on Mauna Kea, a target source observing fraction of 0.67, a wind velocity of 5 m/s, and 1 GHz, 2 GHz, and 10 GHz total (both polarizations combined) bandwidth cases. The 10 GHz curve on this plot is similar to the 1 GHz curve on the 0.33 target source observing fraction plot (Figure 5).

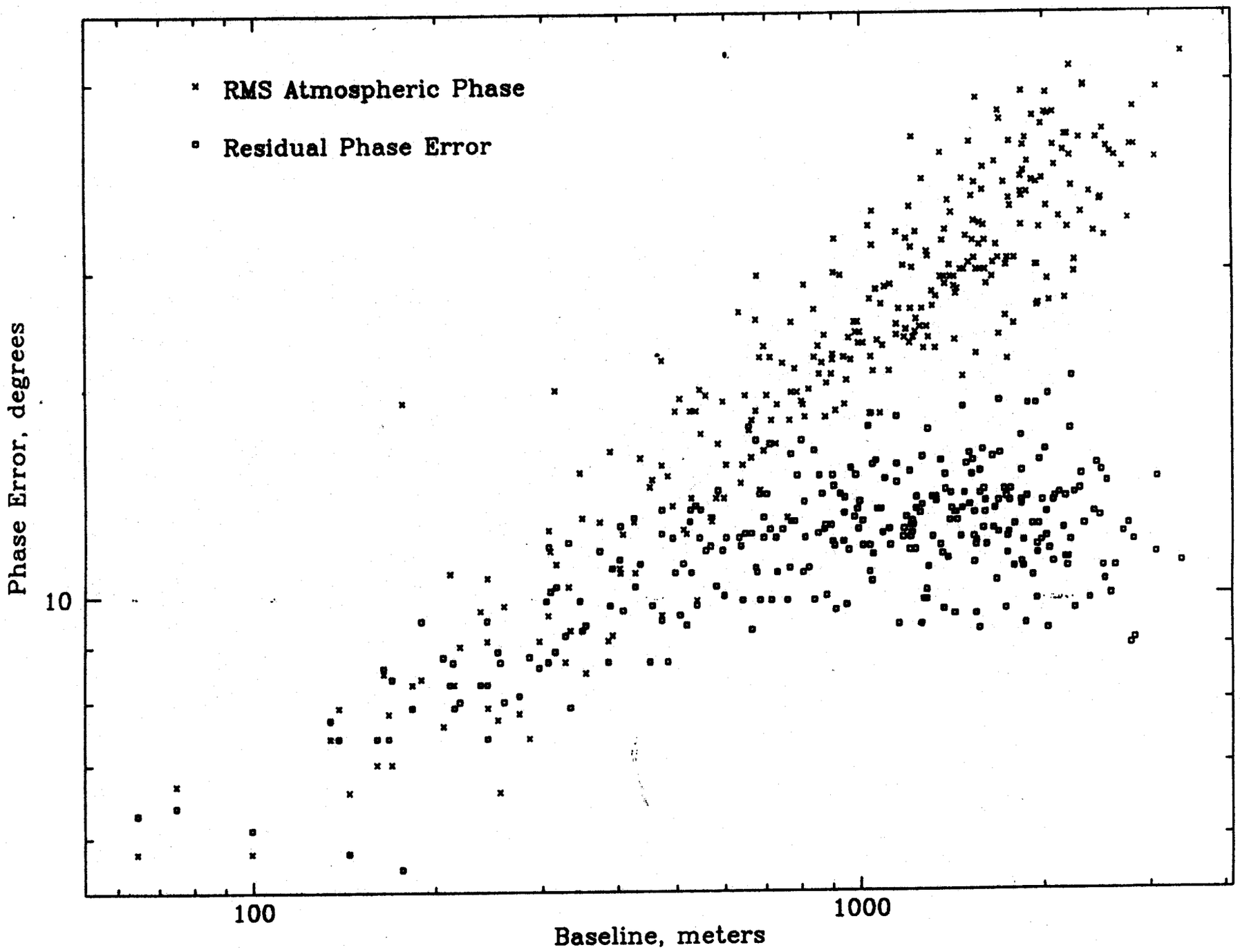
RMS Atmospheric Phase
Residual Phase Error
Phase Error, degrees
10
100
1000
Baseline, meters

Figure 1

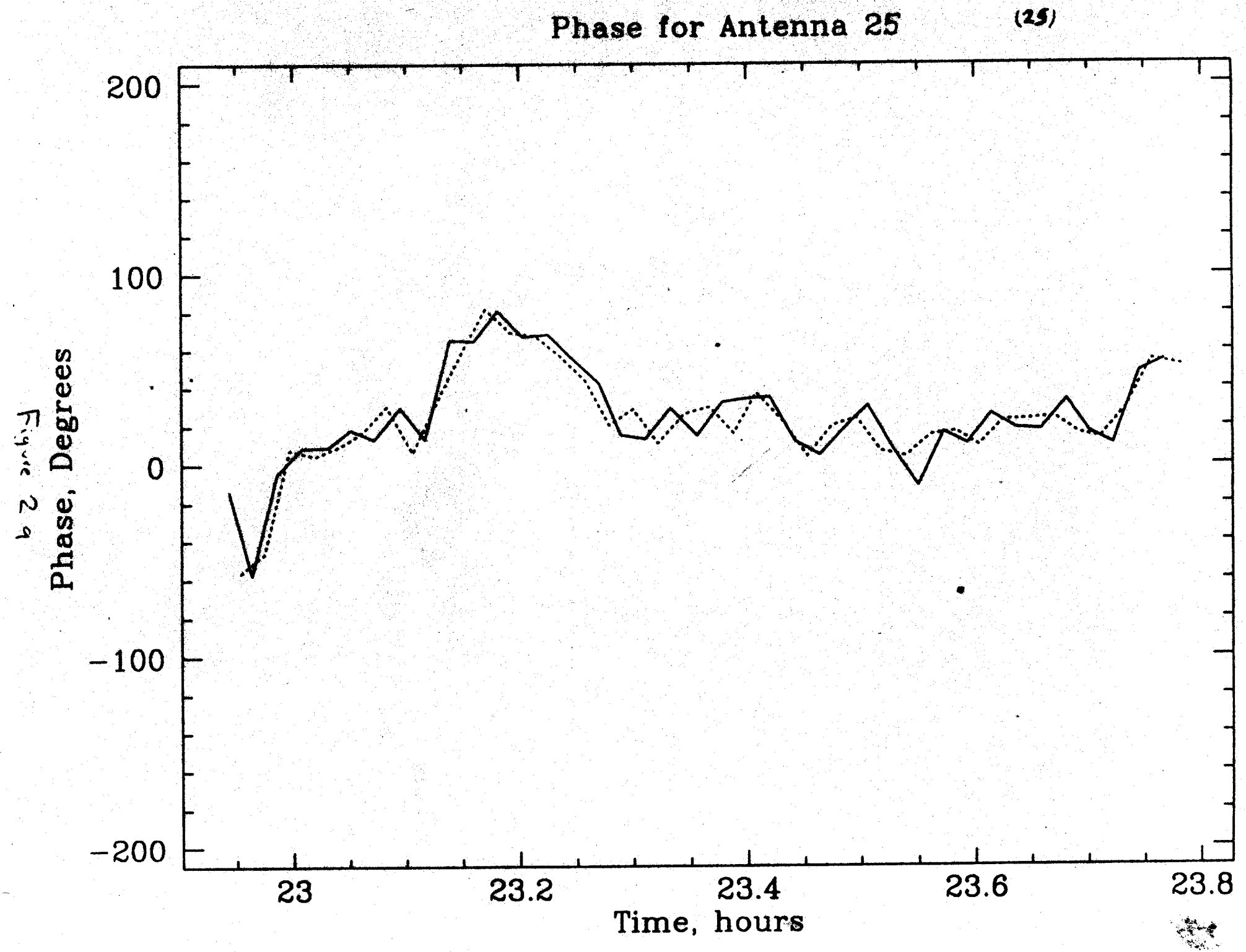
Phase for Antenna 25
200
100
0
−100
−200
Phase, Degrees
23
23.2
23.4
23.6
23.8
Time, hours

Figure 24

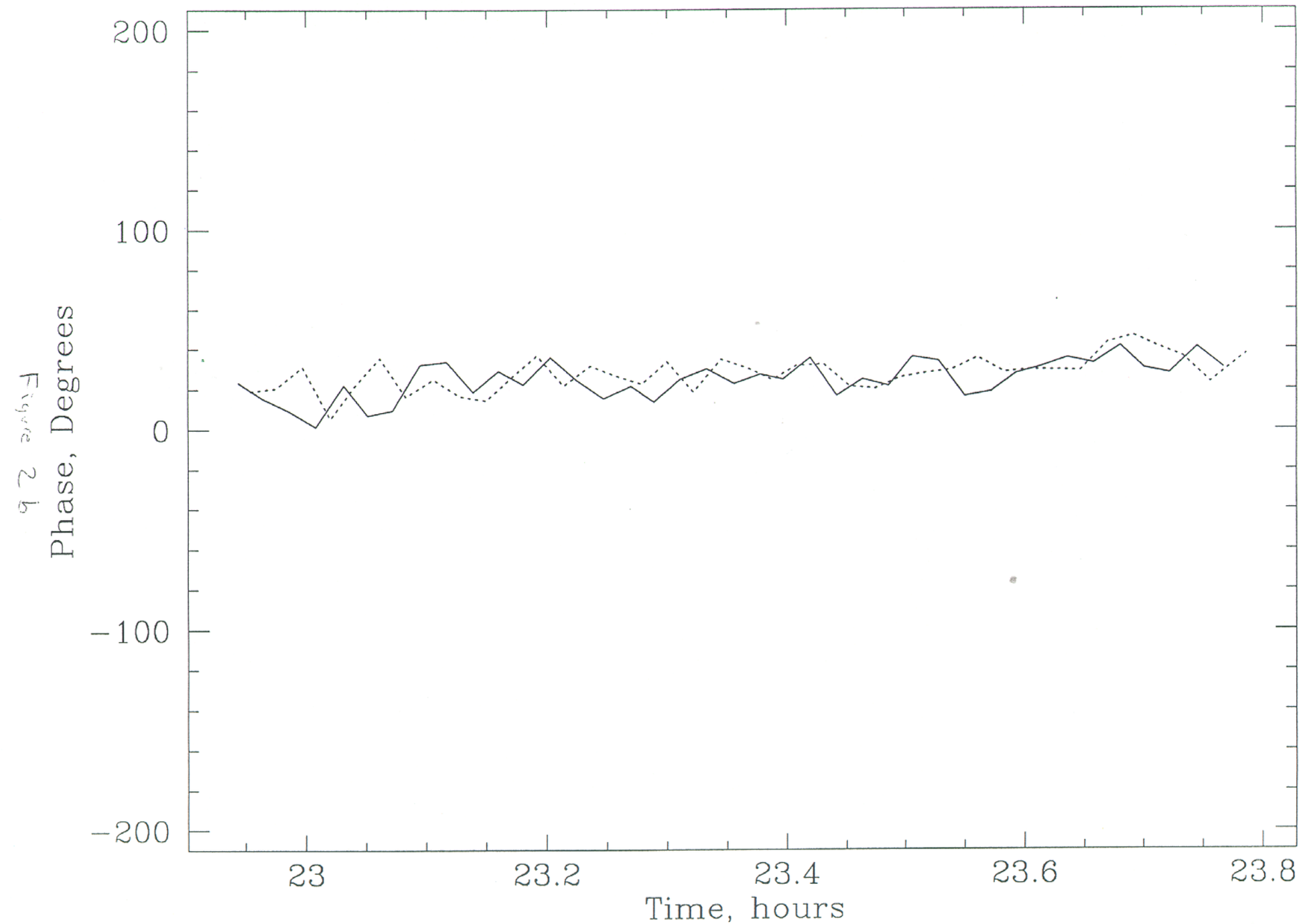
Phase for Antenna 7
200
100
0
−100
−200
Phase, Degrees
23
23.2
23.4
23.6
23.8
Time, hours

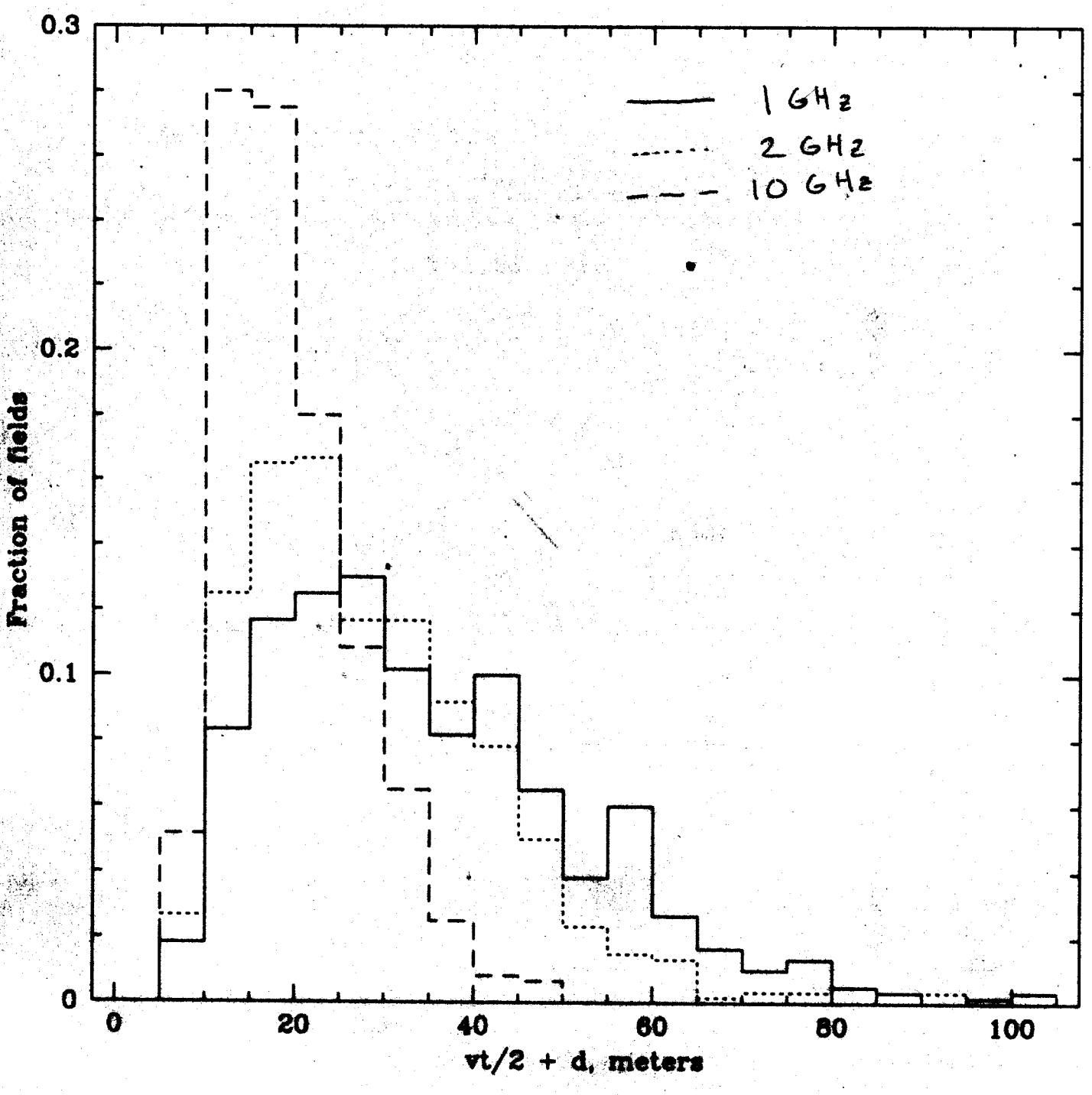
Probability Distribution of vt/2 + d for 1,2,10 GHz, v=5m/s
1 GHz
2 GHz
10 GHz
Fraction of fields
0.3
0.2
0.1
0
0
20
40
60
80
100
vt/2 + d, meters

Figure 3

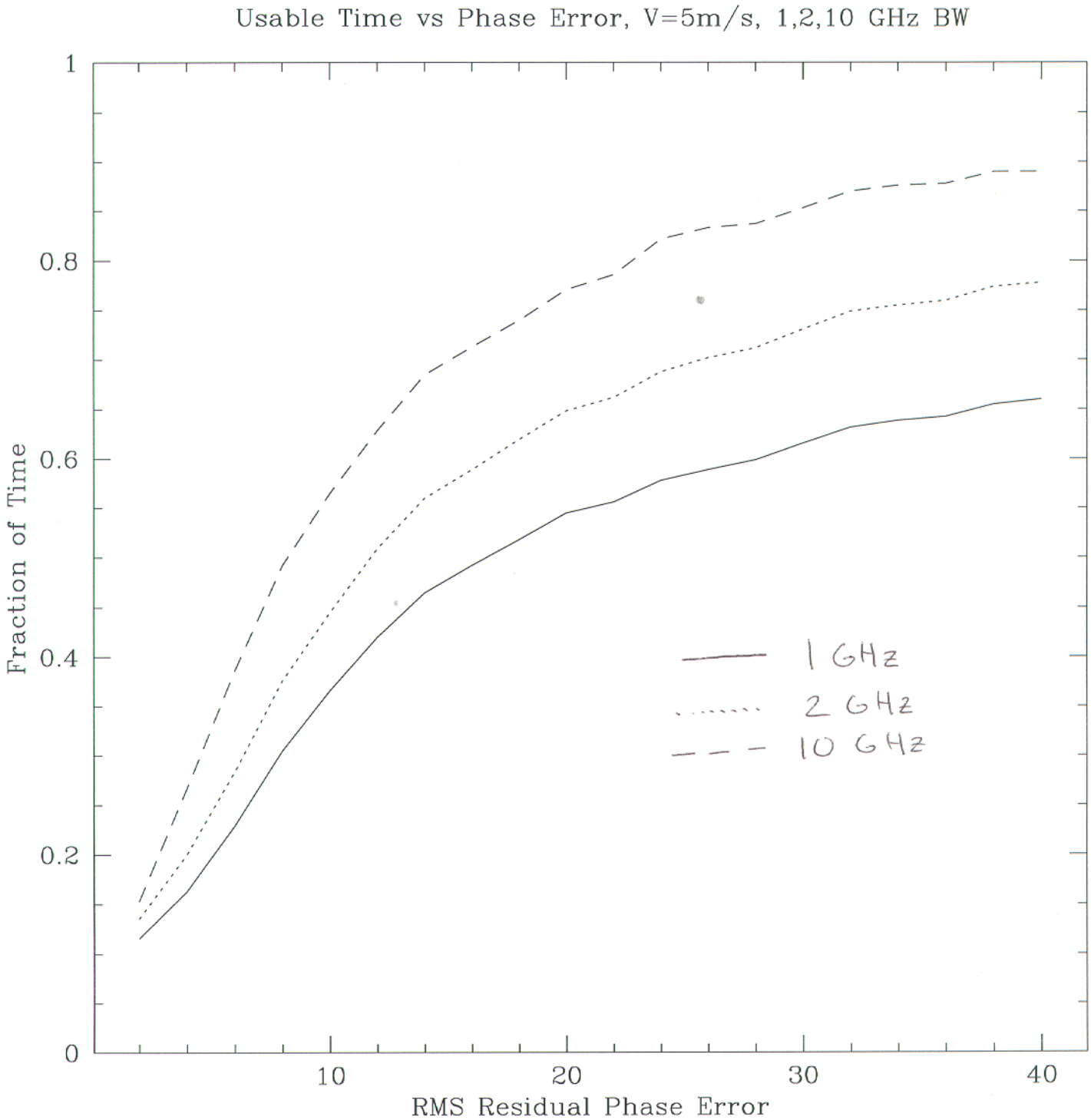
Usable Time vs Phase Error, V=5m/s, 1,2,10 GHz BW
Fraction of Time
RMS Residual Phase Error
0
0.2
0.4
0.6
0.8
1
10
20
30
40
1 GHz
2 GHz
10 GHz

Figure 4

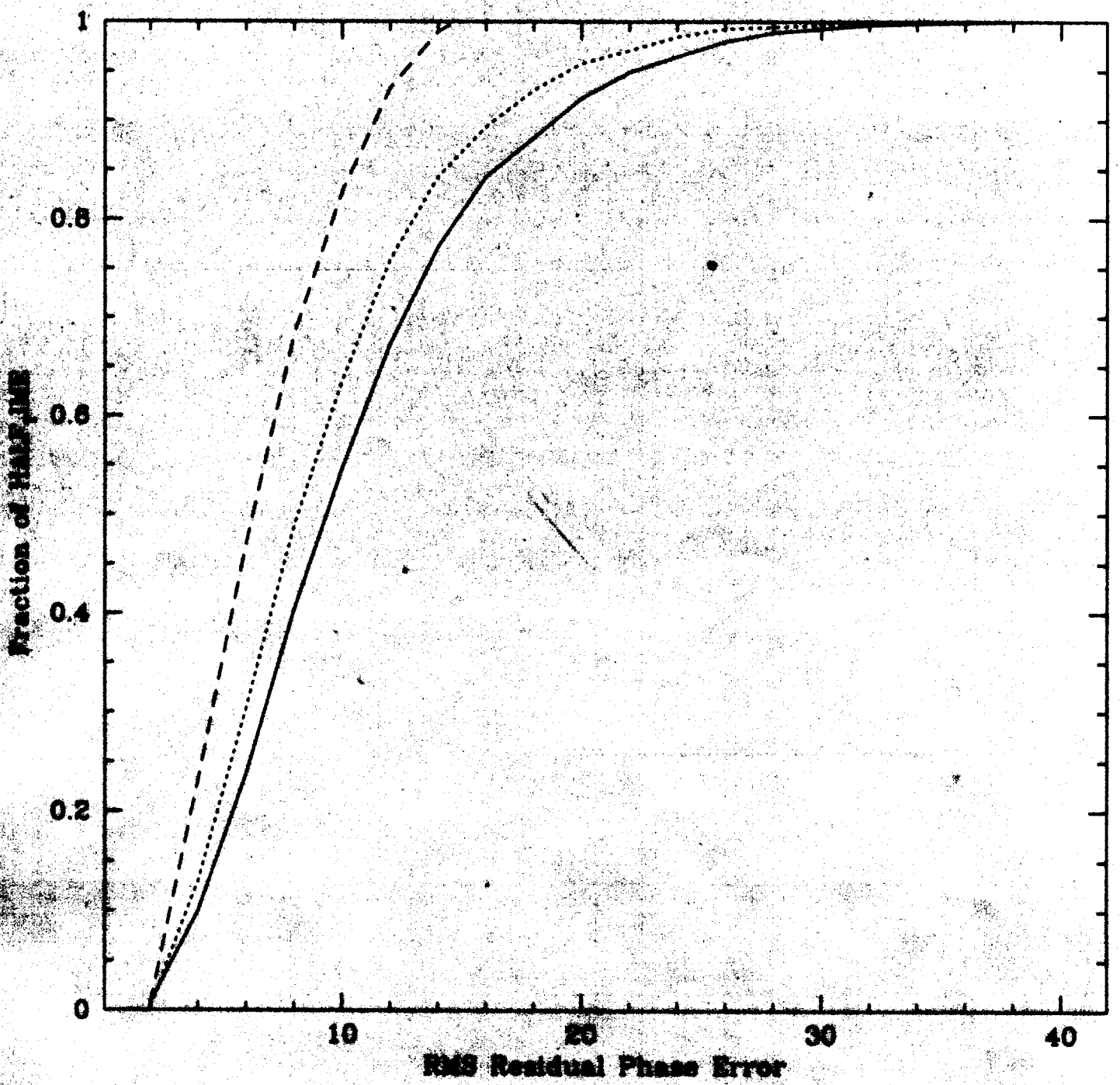
Best Half: Usable Time vs Phase Error, V=5m/s, 1,2,10 GHz BW
1
0.8
0.6
0.4
0.2
0
Fraction of Half Time
10
20
30
40
RMS Residual Phase Error

Figure 5

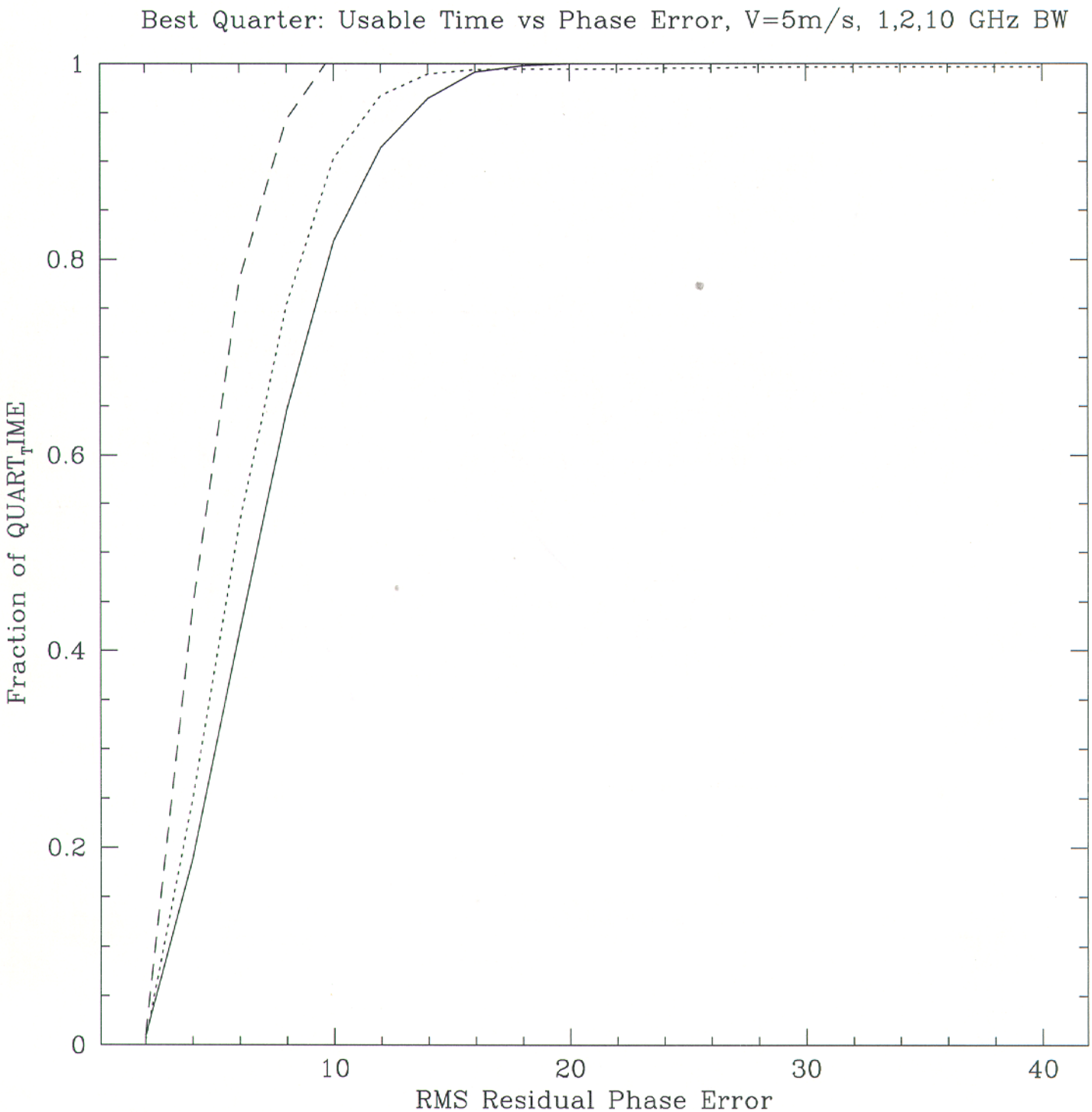
Best Quarter: Usable Time vs Phase Error, V=5m/s, 1,2,10 GHz BW
Fraction of QUART$_T$IME
RMS Residual Phase Error
0
0.2
0.4
0.6
0.8
1
10
20
30
40

Figure 6

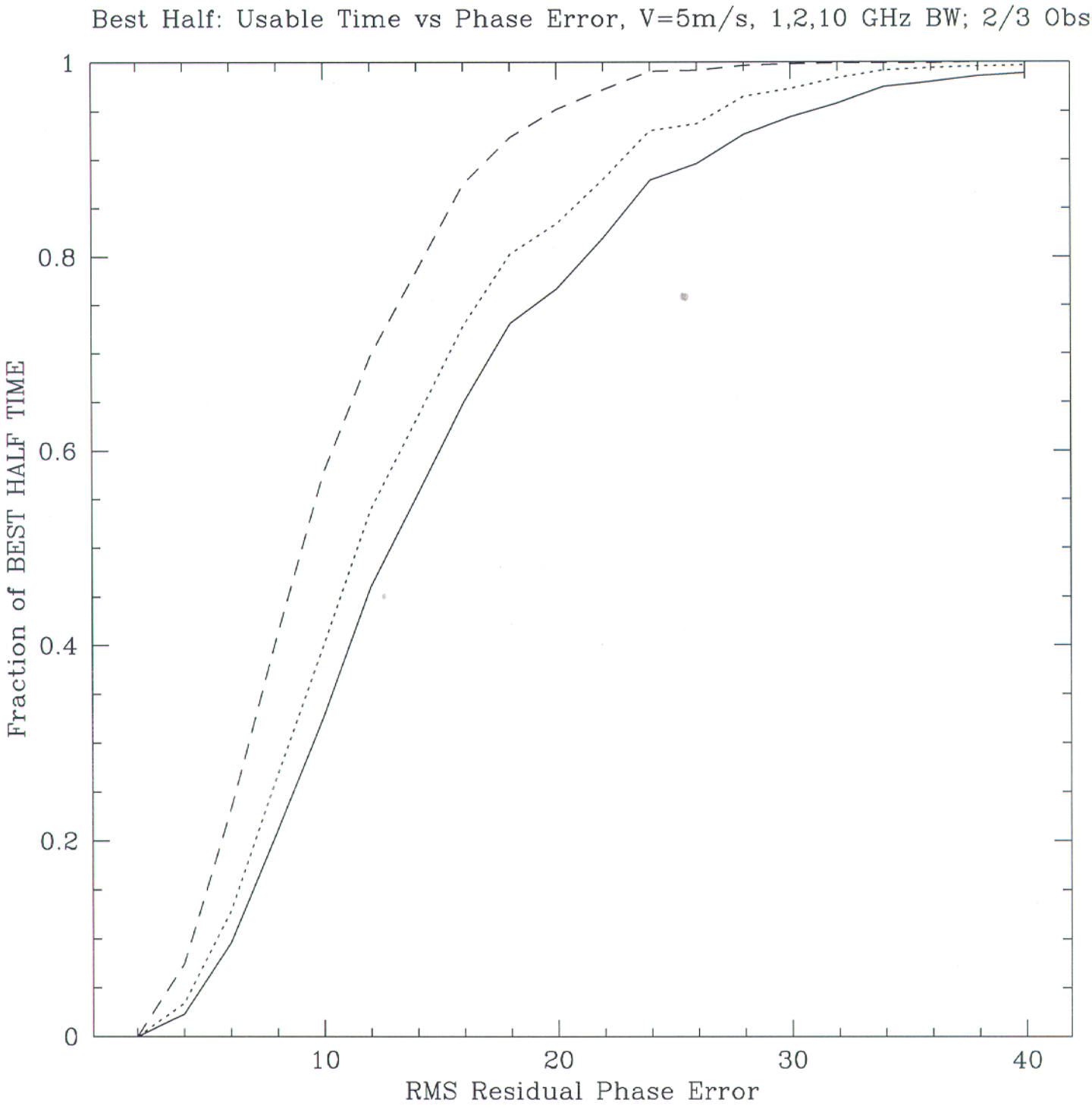
Best Half: Usable Time vs Phase Error, V=5m/s, 1,2,10 GHz BW; 2/3 Obs
Fraction of BEST HALF TIME
RMS Residual Phase Error
0
0.2
0.4
0.6
0.8
1
10
20
30
40

Figure 7